Abdominal Radiology

Published online: 27 February 2018

Abdom Radiol (2018) 43:773–785
https://doi.org/10.1007/s00261-018-1475-6

Principles of ultrasound elastography

Arinc Ozturk,[1] Joseph R. Grajo,[2] Manish Dhyani,[1] Brian W. Anthony,[3] Anthony E. Samir[1]

[1]Center for Ultrasound Research & Translation, Department of Radiology, Massachusetts General Hospital, Boston, MA 02114, USA
[2]Department of Radiology, Division of Abdominal Imaging, University of Florida College of Medicine, Gainesville, FL, USA
[3]Device Realization and Computational Instrumentation Laboratory, Department of Mechanical Engineering, Massachusetts Institute of Technology, Cambridge, MA 02139, USA

Abstract

Tissue stiffness has long been known to be a biomarker of tissue pathology. Ultrasound elastography measures tissue mechanical properties by monitoring the response of tissue to acoustic energy. Different elastographic techniques have been applied to many different tissues and diseases. Depending on the pathology, patient-based factors, and ultrasound operator-based factors, these techniques vary in accuracy and reliability. In this review, we discuss the physical principles of ultrasound elastography, discuss differences between different ultrasound elastographic techniques, and review the advantages and disadvantages of these techniques in clinical practice.

Key words: Ultrasound—Elastography—Shear wave—Strain

Since time immemorial, physicians have gained insight into tissue biology through diagnostic palpation, the physical examination technique by which mechanical tissue property changes are detected. Changes in tissue mechanics typically accompany common disease processes, including fibrosis, inflammation, and neovascularization. These changes can be assessed with new advanced ultrasound techniques, termed ultrasound elastography.

Elastography Physics

Elastography is the set of techniques by which tissue stiffness is estimated as a physical property termed the Young's modulus (E). The Young's modulus is a proportionality constant that relates applied force per unit area or stress, and the resultant relative change in tissue dimension, or strain. Ultrasound elastography methods may be divided into two categories: quasi-static, or strain based, and dynamic, or shear wave based.

The nature of the external mechanical stimulus defines these methods. In strain-based elastography, force is applied by the application of probe pressure or through endogenous mechanical force (e.g., carotid pulsation). In shear wave-based elastography, a tissue shear wave is induced by the imaging system. In both approaches, the response of tissue to these mechanical stimuli is used to estimate tissue mechanical properties. Strain imaging uses the direct relationship $E = \sigma/\varepsilon$ (Hooke's Law) in which σ represents externally applied stress, and ε represents strain [1, 2]. Young's modulus is usually not computed with clinical strain imaging systems, as the applied force on the tissue of interest is usually not known. Shear wave imaging systems compute Young's modulus using the relationship $E = 3\rho c_s^2$ in which ρ represents tissue density, and c_s represents shear wave speed [1, 2]. Most vendors provide automatic calculation systems convert kPa to m/s and m/s to kPa and most ultrasound systems can display a table that indicates stiffness values both in kPa and m/s.

Strain elastography (SE)

SE measures tissue stiffness by applying external tissue pressure [3]. Tissue dimensions change due to the applied pressure; this deformation is termed strain. Stiffer lesions deform less, and have correspondingly lower strain and higher Young's modulus. The strain ratio can be computed as the ratio between strain in a region of tissue and strain in a reference region of tissue. Computation of the strain ratio does not require knowledge of the applied force. For this reason, strain ratio is commonly used in clinical practice, and is mathematically equivalent to the Young's modulus ratio between two tissue regions, assuming applied force is equivalent across these regions.

Correspondence to: Anthony E. Samir; *email:* asamir@mgh.harvard.edu

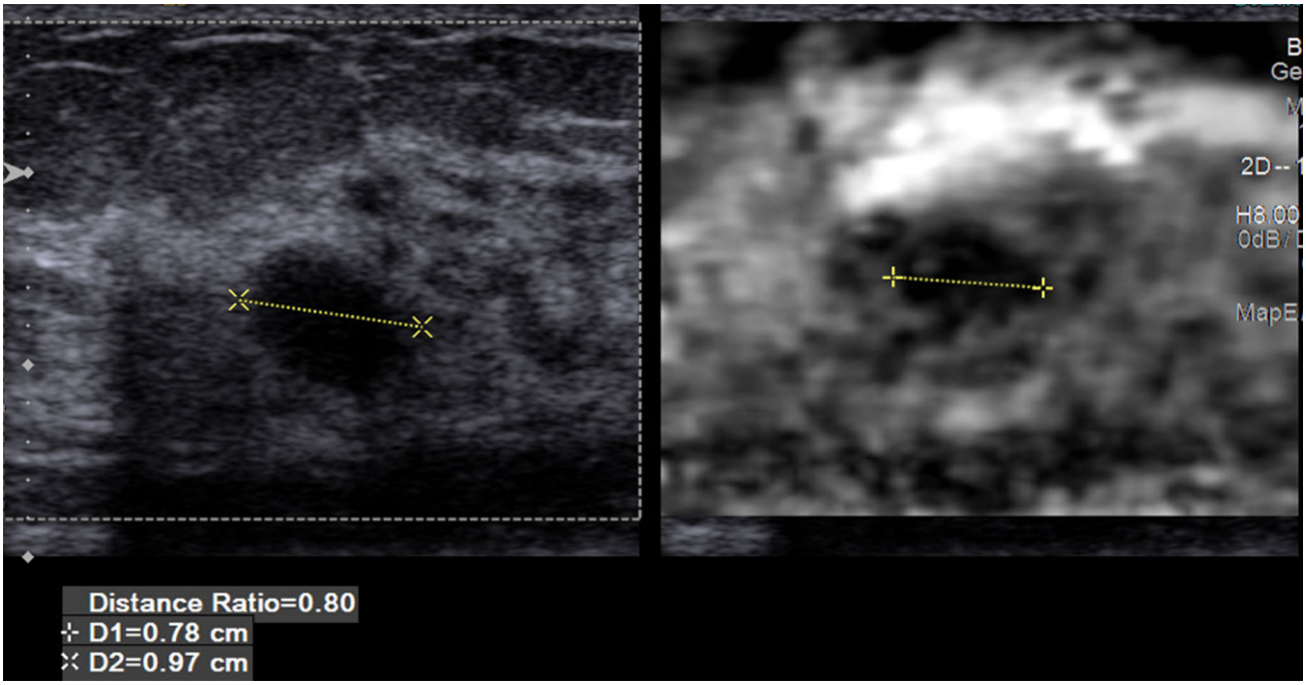

Fig. 1. Palpable breast mass from a 24-year-old woman proven to be a benign fibroadenoma. A conventional B-mode image on the left, and a map of relative tissue stiffness in the same region of interest on the right. On the elastogram, bright areas depict tissue that is less stiff than tissue in the dark areas. Images were acquired using a L9 probe on a Siemens S2000 US system with manual strain (Courtesy of Dr. Richard Barr, MD, PhD).

Strain elastography can be further divided into two groups by the method of tissue excitation (external manual excitation or excitation with internal physiological movement) [1]. Excitation with manual pressure measures elasticity in superficial tissues. A disadvantage of this excitation method is that manual stress is not efficiently transmitted to deeper tissues. Excitation from natural physiologic motion, such as cardiac pulsation and respiration, is another mechanism of generating tissue stress. Deep organs can be assessed with this method [1]. A variety of strain elastography implementations are available on clinical ultrasound systems, including ElaXto™, Real-time tissue elastography™, ElastoScan™, eSie Touch™, and Elasticity Imaging by the manufacturers Esaote, Hitachi, GE, Philips, Toshiba, Ultrasonix, Mindray, Samsung, and Siemens [1, 2]. A strain image example, in comparison with a conventional ultrasound image, is indicated in Fig. 1. In Virtual Touch™ Imaging (VTI), strain elastography is performed with the help of an acoustic push pulse, eliminating the need for an external/internal excitation method [2].

In strain imaging, tissue displacement is calculated by processing radiofrequency (RF) datasets obtained before and after compression [4]. Translucent colored elastograms (strain images) can be superimposed on B-mode images to provide complementary anatomic information. It is common to display the strain map as colored pixels on a red/blue scale or gray scale [5]. Unfortunately, intermanufacturer display scale variability is substantial, limiting inter-vendor comparability of strain elastography images.

Parameters commonly used in strain elastography include:

- Strain ratio measures tissue deformation compared between two regions of interest (ROI). Strain ratio > 1, is an indicator of relatively low strain high stiffness [2].
- Elasticity scores or grading systems are qualitative systems that have been used in a wide spectrum of disease processes, including breast imaging, to assess lesions [5]. These systems typically classify elastography patterns in a range between benign and malignant [1, 5].
- Fat-to-lesion strain ratio is the strain ratio between fat and a lesion [6].
- Elastography-to-B-mode size ratio is an index of the maximum size of a lesion on elastogram to that on a corresponding B-mode image [7].

Generally, in deep organs such as the liver and kidney, tissue stress is obtained with the help of cardiac/arterial or respiratory motion. In superficial organs like the thyroid, tissue stress is obtained with the help of manual compression. A strain image example of a lesion

in comparison with a conventional ultrasound image is presented in Fig. 1.

Shear wave elastography (SWE)

The compressive acoustic waves used for conventional B-mode image generation travel at high speeds through soft tissue (1450–1550 m/s). By contrast, mechanical shear waves used for shear wave elastography travel relatively slowly (1–10 m/s). Shear wave propagation velocity depends on tissue stiffness [2, 4]. In commercially available shear wave elastography systems, compressive acoustic waves are used both to induce and track shear waves. Acoustically induced shear waves travel perpendicular to compressive waves; tissue motion induced by these shear waves is monitored at multiple locations along the ultrasound probe, permitting shear wave velocity estimation [4]. Young's modulus can be algebraically derived from the shear wave speed (SWS).

SWE can be used in many different tissues for a variety of applications including hepatic lesion characterization [8], renal lesion characterization [9], diffuse liver and renal disease evaluation [10, 11], breast mass diagnosis [12, 13], prostate cancer detection [14], thyroid lesion characterization [15], and tendon imaging [16].

Transient elastography (TE)

A low-frequency (50 Hz) mechanical push is generated by a mechanical actuator and a resulting shear wave is generated and evaluated [17, 18]. With this technique, parameters like anisotropy, viscosity or elastic non-linearity can also be obtained [19]. Shear wave propagation velocity is proportional to tissue stiffness, which increases with fibrosis [20]. 1D transient elastography is marketed under the trade name FibroScan®. TE measures tissue stiffness over a 1 cm diameter–4 cm length region of tissue, which is 100 times larger than that evaluated with liver biopsy. If the pulse is not transmitted and recorded successfully, the software does not provide a reading [21]. Stiffness values are presented in kPa. Controlled Attenuation Parameter (CAP), is a technology that quantifies hepatic steatosis by measuring the energy loss as the sound wave passes through the medium. Total attenuation at 3.5 MHz is expressed in dB/m and steatosis is estimated using the same radiofrequency data as elastography, in the same location that stiffness is measured [22] (Fig. 2).

Point shear wave elastography (pSWE)

Focused ultrasound results in focal tissue displacement, a process termed acoustic radiation force impulse (ARFI) imaging. The resultant shear waves are tracked, yielding a shear wave speed estimate that is an algebraic function of tissue stiffness. Point SWE is available on the Siemens

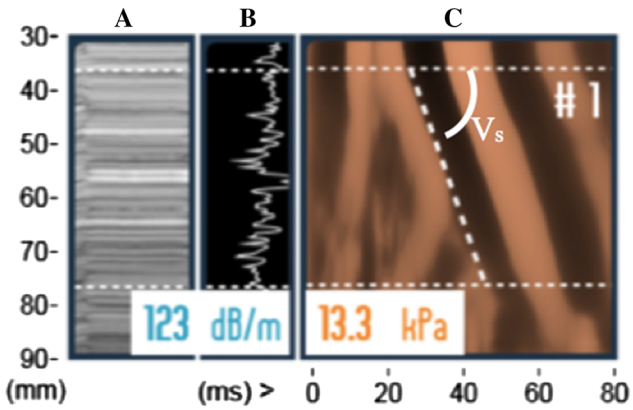

Fig. 2. Transient elastography acquisition on a phantom. **A** Time Motion (TM) mode **B** Amplitude (A) mode. TM and A modes are used to locate ideal liver part. **C** Shear wave propagation image. *y*-axis is distance from skin, *x*-axis is time. Slope of the dashed line is shear wave speed (V_s) [23]. Tissue stiffness value is indicated in kPa. In the left panel, controlled attenuation parameter (CAP) value, which quantifies steatosis level, is indicated in dB/m.

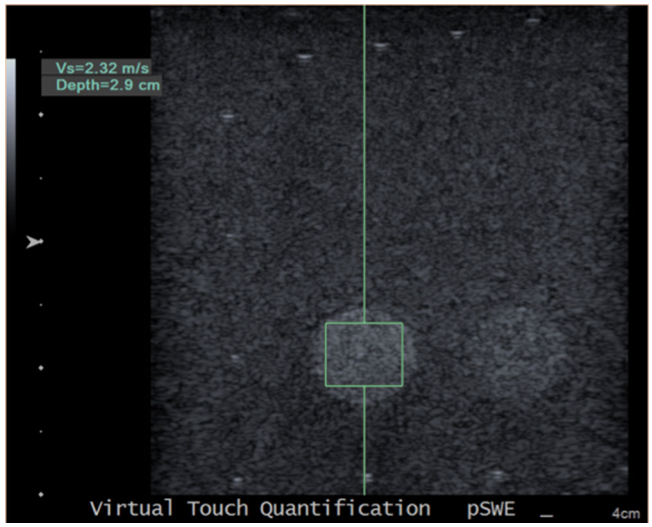

Fig. 3. pSWE acquisition in a phantom. Green box is the focus of ARFI excitation. Shear wave speed value is indicated in left panel.

Virtual Touch™ Quantification (VTQ/ARFI) system and on the Philips ElastPQ™ system [2]. An example of pSWE application in a phantom is presented in Fig. 3.

2D shear wave elastography

In this technique, acoustic radiation force is used to displace tissue at multiple points. The resultant shear wave front is readily detectable with high frame rate imaging, which is used to monitor propagation of the shear waves in real time at multiple points in the image [24]. A quantitative elasticity image (elastogram) is pre-

sented as a colorized display map, with quantitative results available as shear wave propagation speed in m/s or as the algebraically derived Young's modulus in kPa [25]. Real-time tissue stiffness color maps added to the B-mode image allows the operator to avoid confounding anatomic structures such as blood vessels [26]. Maximum elastogram sizes are 2–3 cm in side length with a linear probe, and 9 × 4 cm with a convex probe [24]. This technique is available on multiple ultrasound systems including Virtual Touch™ Imaging Quantification (VTIQ/ARFI) by Siemens, Shear Wave Elastography by Philips, Shear Wave™ Elastography by SuperSonic Imagine, 2D-SWE by GE Healthcare, and Acoustic Structure Quantification™ (ASQ) by Toshiba [2]. An example of 2D-SWE in a phantom is presented in Fig. 4.

Clinical applications

Liver

Strain elastography

The liver fibrosis index (LFI) [27, 28] has been shown to be an accurate technique to distinguish fibrosis stages with AUROC (Area under receiver operating characteristic) values of 0.82 for fibrosis stage F0–1 vs. F2–4 and 0.87 for fibrosis stage F0–3 vs. F4 [27]. Koizumi et al. reported that a different strain parameter, termed 'elastic ratio' (the strain distribution value, intrahepatic venous small vessels/value in the hepatic parenchyma), was highly correlated with biopsy-proven fibrosis stage (Spearman correlation 0.82) with AUROC values to diagnose $F \geq 2$ (0.89), $F \geq 3$ (0.94), and $F = 4$ (0.95) [29]. SE can also be used to evaluate liver masses, with significant differences reported between benign and malignant lesions [30].

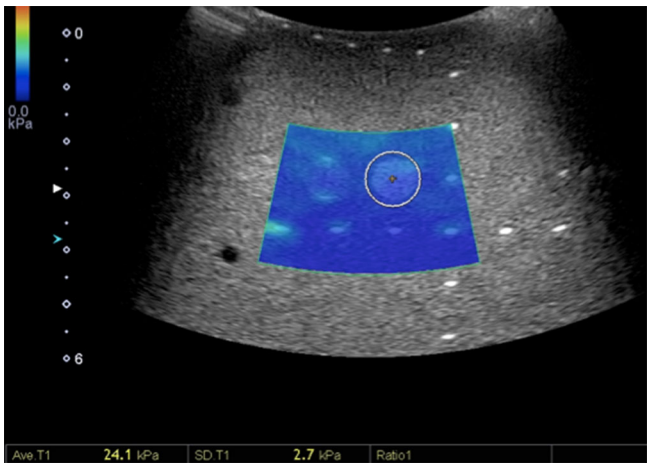

Fig. 4. 2D-SWE acquisition in a phantom. Blue box denotes elastographic field of view (FOV) and circle decodes region of interest. Tissue stiffness in kPa is indicated at the bottom of the image. The color scale can be adjusted by the user. Blue areas are less stiff than red areas.

Transient elastography

Transient elastography can be used in the diagnosis of liver fibrosis due to multiple etiological factors including chronic viral infection and excessive alcohol intake [31–33]. In a meta-analysis including chronic liver disease due to multiple etiological factors, TE showed summary sensitivity and specificity values of 0.79 (95% CI 0.74–0.82) and 0.78 (95% CI 0.72–0.83) for F2 stage and 0.83 (95% CI 0.79–0.86) and 0.89 (95% CI 0.87–0.91) for cirrhosis [34]. TE does not use B-mode anatomic imaging to define the tissue from which stiffness information is obtained. The operator uses A-Mode US to define a measurement location away from vascular structures [2]. Therefore, an operator is not able to select the same liver region for serial TE measurements over time. Obtaining reliable acquisitions requires (1) at least 10 valid measurements, (2) valid measurements/total measurements ratio ≥ 60%, and (3) interquartile range (IQR) less than 30% of median value. A short training period is typically required for TE operators [2, 35]. TE has been shown to be reproducible with inter-operator intraclass correlation coefficient (ICC) of 0.98 and intra-operator ICC of 0.98 [36]. CAP is an integrated technology which can be used simultaneously with liver fibrosis quantification in Fibroscan system. An image example of transient elastography is depicted in Fig. 5.

pSWE

pSWE can be used in HBV, HCV, hepatic toxicity, alcoholic liver disease, and autoimmune hepatitis-related liver fibrosis [37–39]. It can also be used as a screening tool for early stage fibrosis detection [40], although evidence of benefit in this setting is limited. pSWE has been shown to be useful in detection of liver fibrosis. In a recent meta-analysis of 23 studies, Hu et al. reported AUROC values to distinguish liver fibrosis stages ranging from 0.649 to 0.934 for $F \geq 2$, 0.848 to 0.97 for $F \geq 3$, and 0.723 to 0.98 for F4 [41]. Using point SWE technique on both the liver and spleen has greater discriminative power than assessment of the liver alone [42]. Setting the ROI away from the liver capsule is recommended, as this choice results in more reliable shear wave speed values [43]. pSWE is a reproducible and reliable liver stiffness assessment technique, with ICC values of 0.89 (95% CI 0.85–0.92) for intra-observer and 0.85 (95% CI 0.76–0.90) for inter-observer agreement [44]. An image example of pSWE is demonstrated in Fig. 5.

2D-SWE

2D-SWE is a useful and feasible technique for fibrosis staging in both pediatric and adult patients [10, 45]. 2D-SWE has good performance for fibrosis staging. For example, for the diagnosis of fibrosis stage $F \geq 2$,

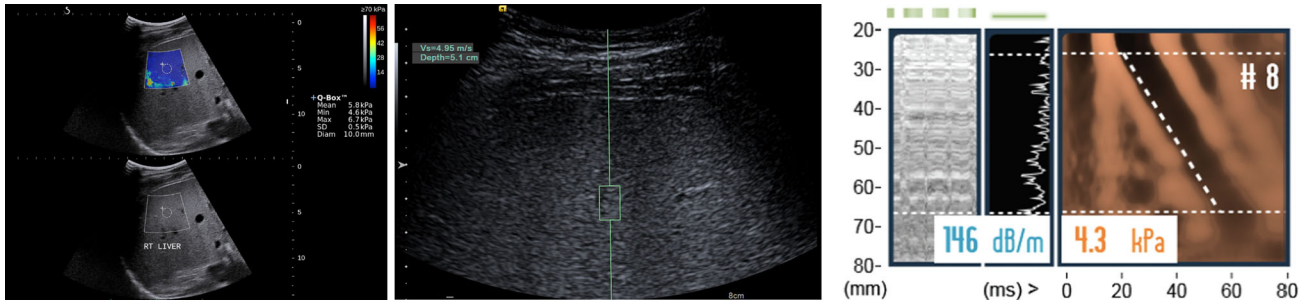

Fig. 5. Liver elastography image examples: (1) 2D-SWE acquisition of liver with Supersonic Aixplorer. Color-coded elastogram with color scale on right top. SWE values are indicated below the scale. (2) pSWE acquisition of liver with Siemens ACUSON S3000. ARFI-induced technique measures SWS in the center area. (3) Transient Elastography measurement example with Fibroscan.

AUROC of 0.862 has been reported, and for early cirrhosis diagnosis, AUROC of 0.926 has been reported [46]. Using a cut-off value 7.29 kPa, this technique reaches a sensitivity of 95.4% for fibrosis stage ≥ 2 [47]. Although the diagnostic ability of the techniques is similar, shear wave speed values obtained from 2D-SWE may show higher stiffness values [48]. An image example of 2D-SWE is depicted in Fig. 5.

Kidney

Strain elastography

Chronic kidney disease (CKD) patients have been reported to show higher strain index (ratio) values when compared to healthy volunteers [49]. SE can also be used to detect renal graft interstitial fibrosis, a manifestation of organ rejection as a long-term complication of renal transplantation. Early diagnosis of graft fibrosis may play a useful role in treatment decisions concerning immunosuppressive agents [50].

pSWE

Renal fibrosis and diabetic renal disease can be evaluated with pSWE techniques. pSWE can detect renal fibrosis with a sensitivity of 86.3% and specificity of 83.3% [51]. Yu et al. reported a correlation of 0.773 between urinary albumin-to-creatinine ratio (diabetic kidney disease marker) and shear wave speed determined by VTQ, implying pSWE may serve as a marker for diabetic kidney disease [52]. Renal pSWE has been shown to be moderately reliable with intraclass correlation coefficient (ICC) values of 0.71 in the right kidney and 0.69 in the left kidney [53]. Age and gender can influence the SWS measurements acquired from the kidney [54, 55].

2D-SWE

2D-SWE can be used to diagnose chronic kidney disease. CKD patients show higher stiffness values [9.4 kPa] when compared with healthy volunteers [4.4 kPa] [11]. 2D-SWE can also be used in the diagnosis of diabetic kidney disease (DKD). Hassan et al. reported a significant difference in cortical stiffness values of DKD patients and healthy subjects (23.7 kPa vs. 9.02). Furthermore, significant differences between CKD grades have been reported [56]. An image example of 2D-SWE in renal tissue is demonstrated in Fig. 6.

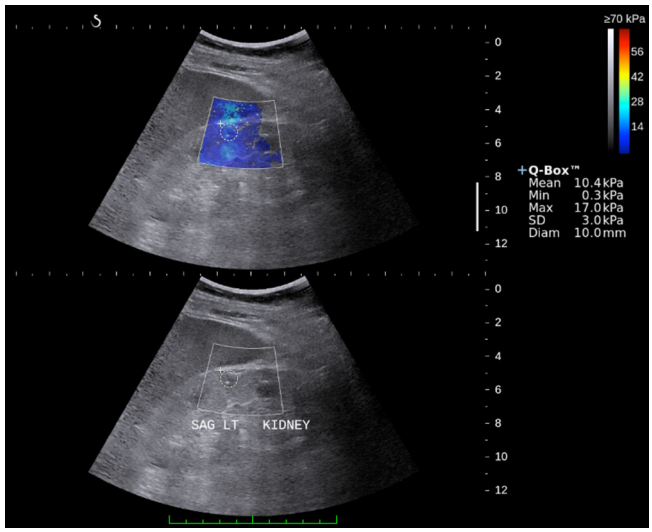

Fig. 6. 2D-SWE image of kidney. Mean stiffness is 10.4 kPa for this patient, likely reflecting elevated renal stiffness due to CKD-related fibrosis [11].

Breast

Strain elastography

Several *strain elastography* features have been proposed, including strain ratio, elasticity score (Tsukuba score), and elastography-to-B-mode size ratio [57]. In a meta-analysis with 25 studies focusing on elasticity score and strain ratio, overall mean sensitivity and specificity values to diagnose malignant breast lesions were reported as 0.834 (95% CI 0.814–0.853) and 0.842 (95% CI

0.829–0.854), respectively, for elasticity score and 0.883 (95% CI 0.844–0.916) and 0.814 (95% CI 0.786–0.839) respectively, for strain ratio [58]. Furthermore, tumor grade may also be distinguished using an elasticity imaging/B-mode ratio [59]. It has been shown that the addition of strain elastography to a conventional gray scale ultrasound-based classification system—Breast Imaging Reporting and Data System (BI-RADS)—yields an AUROC of 0.875 for cancer detection with the ability to characterize lesions < 2 cm [60]. Breast lesion size prediction has been reported to be more accurate on elastographic images than conventional gray scale images when compared with the reference standard of the surgical excision specimen [61].

pSWE

Li et al. reported the diagnostic performance of pSWE to differentiate malignant and benign lesions in a meta-analysis of 11 studies, finding an overall sensitivity of 0.84 (95% CI 0.81–0.87) and specificity of 0.94 (95% CI 0.91–0.94) [62]. 2D-SWE and pSWE had similar performance to detect malignancy in breast tissue. In a different meta-analysis of 9 studies comparing 2D-SWE and pSWE, overall sensitivity and specificity values were reported as 0.91 (95% CI 0.88–0.94) and 0.82 (95% CI 0.75–0.87) for 2D-SWE and 0.89 (95% CI 0.81–0.94) and 0.91 (95% CI 0.84–0.95) for pSWE, respectively [63].

2D-SWE

2D-SWE is useful for differentiating benign and malignant breast lesions with reported AUROC values ranging from 0.74 to 0.98 [64]. The addition of 2D-SWE to conventional B-mode ultrasound can improve diagnostic performance by reducing the need for follow-up exams of patients with BI-RADS 3 breast lesions [61].

Prostate

Conventional screening and diagnostic methods for prostate evaluation include Prostate-Specific antigen (PSA) assessment, digital rectal exam (DRE), and transrectal ultrasound (TRUS)-guided biopsy. However, the limited capacity of these techniques to accurately localize prostate cancer has led to the emergence of elastography as a tumor localization technique [65]. Elastographic techniques can be used to assess both benign prostatic hyperplasia (BPH) and prostate cancer (PC).

Strain elastography

In *strain elastography*, images are obtained with slight transrectal manual compression. An inflatable endorectal balloon may be used to generate endorectal prostate elastography images [61]. Although SE-guided prostate biopsy shows higher sensitivity when compared to conventional gray scale US-guided biopsy to detect prostate cancer (60.8% vs. 15%, respectively), only relying on SE results is not recommended [66]. Strain elastography has been shown to have a sensitivity of 58.8% and specificity of 43.3% to identify the prostate cancer index lesion (the main lesion responsible for possible metastasis) [61, 67]. An image example of strain elastography for prostate cancer diagnosis is shown in Fig. 7.

pSWE

In pSWE, malignancy shows higher SWS values than BPH and normal prostate tissue(2.37, 1.98, and 1.34 m/s, respectively) [68]. pSWE can be used to differentiate BPH and malignancy with an AUROC value of 0.86. SWS differences between the transition and peripheral zones of the prostate are possible in both BPH and cancer. When compared to DRE, pSWE shows higher diagnostic accuracy to detect malignancy, with AUROC value of 0.86 (vs. 0.67 for DRE) [68].

2D-SWE

2D-SWE has been shown to be useful for differentiating benign and malignant lesions in the peripheral zone [69]. Using a cut-off stiffness value of 35 kPa to differentiate benign and malignant lesions yields sensitivity and specificity values of 96% and 85%, respectively [70]. 2D-SWE is a reproducible technique with ICC value of 0.876 [71]. In a recent meta-analysis with 7 studies, Sang et al. reported pooled sensitivity and specificity values of 0.844 (95% CI 0.69–0.92) and 0.86 (95% CI 0.79–0.908) (AUROC value of 0.91) to differentiate malignant prostate lesions [72]. A different research group, Woo et al., reported similar results in their recent meta-analysis with 8 studies, pooled sensitivity value of 0.83 (95% CI 0.66–0.92), and specificity value of 0.85 (95% CI 0.78–0.9) [73]. 2D-SWE can also be used to assess BPH. Unlike most prostate malignancies, BPH develops from the transition zone of the prostate. Stiffness values of the transition zone can be measured via transrectal elastography. 2D-SWE can diagnose BPH with an AUROC value of 0.826 (95% CI 0.717–0.934) [74].

Thyroid

Strain elastography

Strain elastography requires external manual compression or physiological motion such as carotid pulsation [75]. The reported sensitivity of different strain imaging features for diagnosis of thyroid carcinoma ranges from 82% to 100%, with specificity ranging from 81.1% to 100% [76]. Although most studies indicate higher accuracy for thyroid cancer detection with strain elastography than conventional gray scale US, there is presently insufficient agreement among research groups regarding

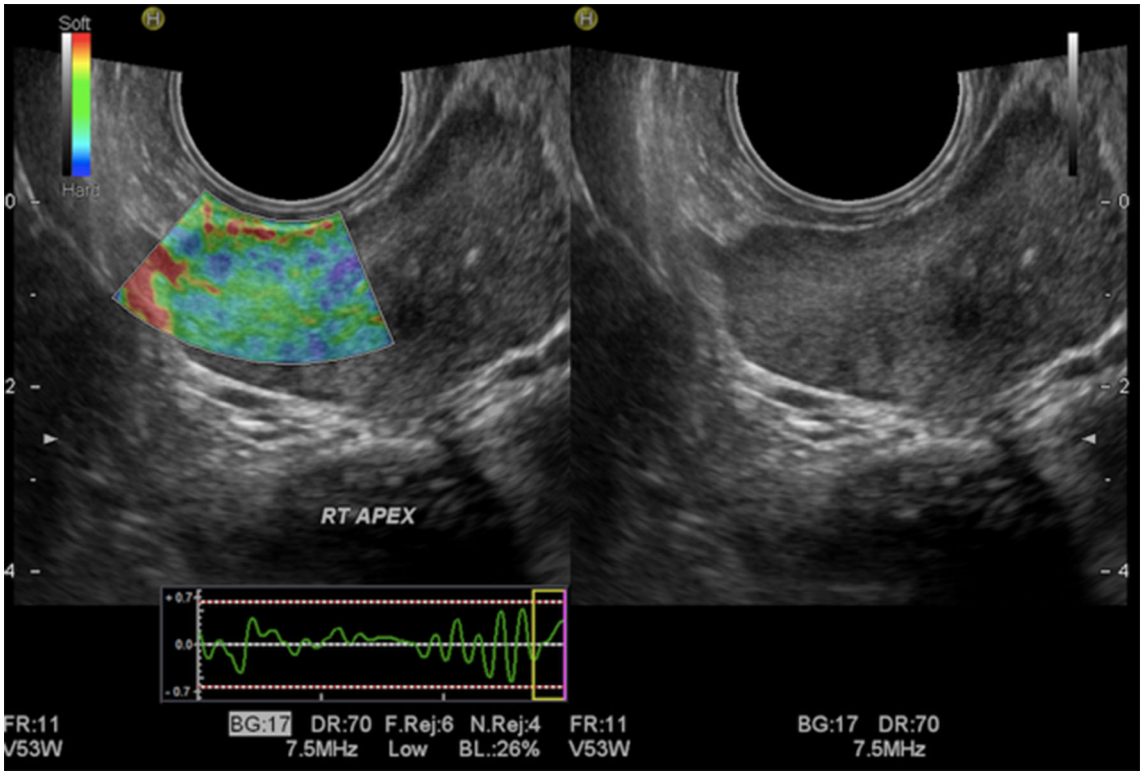

Fig. 7. Transrectal strain image of prostate with distribution of tissue deformation as a colorized map. Blue represents relatively hard tissue and red represents relatively soft tissue. Real-time display of applied compression measured by a force sensor is depicted in the lower part of the image.

diagnostic criteria, and elastography is thought to be insensitive to some malignant tumor types [61, 76–78].

pSWE

Malignant thyroid nodules show higher SWS values when compared to benign nodules, either with pSWE or 2D-SWE [61]. pSWE can differentiate benign and malignant thyroid nodules. In a meta-analysis with 16 studies, pSWE has been reported to have an overall AUROC value of 0.91 [79]. In the assessment of diffuse chronic thyroid disease, pSWE is also useful to differentiate subjects with Graves' disease and autoimmune thyroiditis from healthy subjects [80]. However, this is based on preliminary results and more studies are needed.

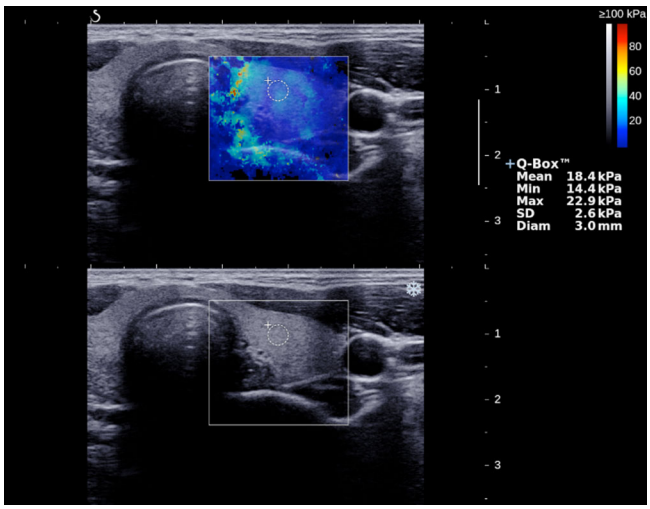

Fig. 9. Summary and classification of elastography techniques.

2D-SWE

2D-SWE is an effective technique to diagnose thyroid malignancies with AUROC values of 0.73 in nodules < 10 mm, 0.88 in nodules 11–30 mm, and 0.82 in nodules > 30 mm [81]. 2D-SWE has also been shown to potentially be able to differentiate benign and malignant follicular thyroid nodules, a clinically relevant finding that cannot be accomplished with FNA [15]. Figure 8 depicts 2D-SWE of normal thyroid tissue. Use of elastographic methods in combination with B-mode ultrasound is recommended [82]. Addition of CEUS can also increase diagnostic performance [83].

Pancreas

Either strain or shear wave elastography can be used in the evaluation of the pancreas. Strain elastography is

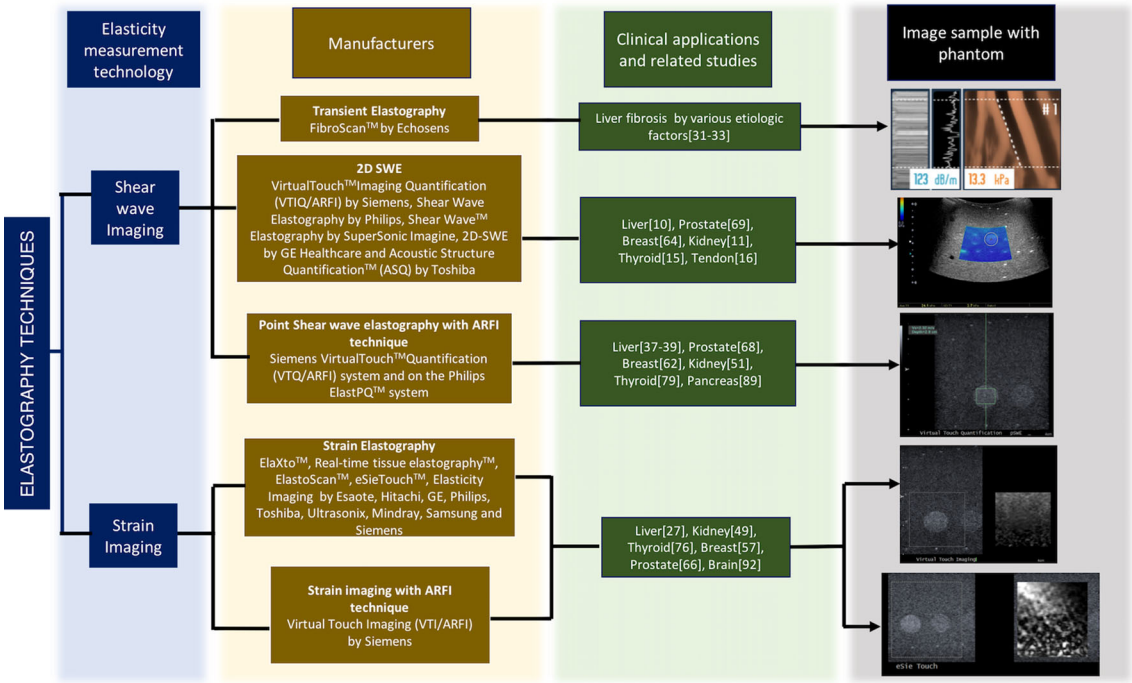

Fig. 9. Summary and classification of elastography techniques.

performed by using an endoscopic ultrasound system, in which aortic pulsation is used as the excitation method. Strain elastography with endoscopic ultrasound is limited by invasiveness, inadequate quality of images from the head and tail of the pancreas, and atherosclerotic changes that can affect aortic pulse excitation. Despite these limitations strain elastography has been used in a number of research studies to assess malignancy and pancreatic parenchymal disease [84].

Strain elastography

In a recent study of 149 patients, Rustemovic et al. proposed a strain ratio cut-off value of 7.59 to distinguish malignancies[100% sensitivity, 95% specificity] [85]. However, previous studies reported different results, which may be caused by the operator dependence of endoscopic ultrasound [84]. In a large mixed study population with 555 subjects that included healthy subjects, patients with chronic pancreatitis and patients with pancreatic cancer, Kim et al. reported mean strain ratio values of 3.78, 8.21, and 21.8, respectively. Sensitivity and specificity to distinguish malignancy were similar as Rustemovic et al.'s results [95.6% and 96.3%, respectively, cut-off 8.86] [86]. In their study with 191 patients with chronic pancreatitis, Iglesias-Garcia et al. reported sensitivity and specificity values of 91.2% and 91%, to detect chronic pancreatitis [AUROC value of 0.949], which are higher than Kim et al.'s values [87].

pSWE

pSWE can be used with cutaneous approach and it can detect stiffness differences between a lesion and background pancreatic parenchyma [88]. D'Onofrio et al. reported significant differences between SWS values obtained in adenocarcinoma and normal pancreatic parenchyma [89]. Patients with chronic pancreatitis may show higher stiffness values with pSWE when compared to healthy controls [4.3 vs. 2.8 kPa] [90]. Current knowledge of pancreatic elastography is limited to strain elastography and pSWE. Studies comparing elastography methods in the diagnosis of pancreatic masses and parenchymal diseases are also limited [91].

Spleen

Portal hypertension and increased hepatic venous pressure gradient (HVPG) are indicators of end-stage chronic liver disease, with increased risk of variceal bleeding, ascites variceal bleeding, ascites, and hepatic encephalopathy which increase mortality rates [2]. Accurate and fast detection of portal hypertension and esophageal varices, is critical to prevent complications, in which elastography techniques may fulfill this need. As mentioned above, strain elastography needs an excitation/pressure method. The spleen is in a relatively deep subcostal location, limiting utility of strain elastography for splenic assessment [61].

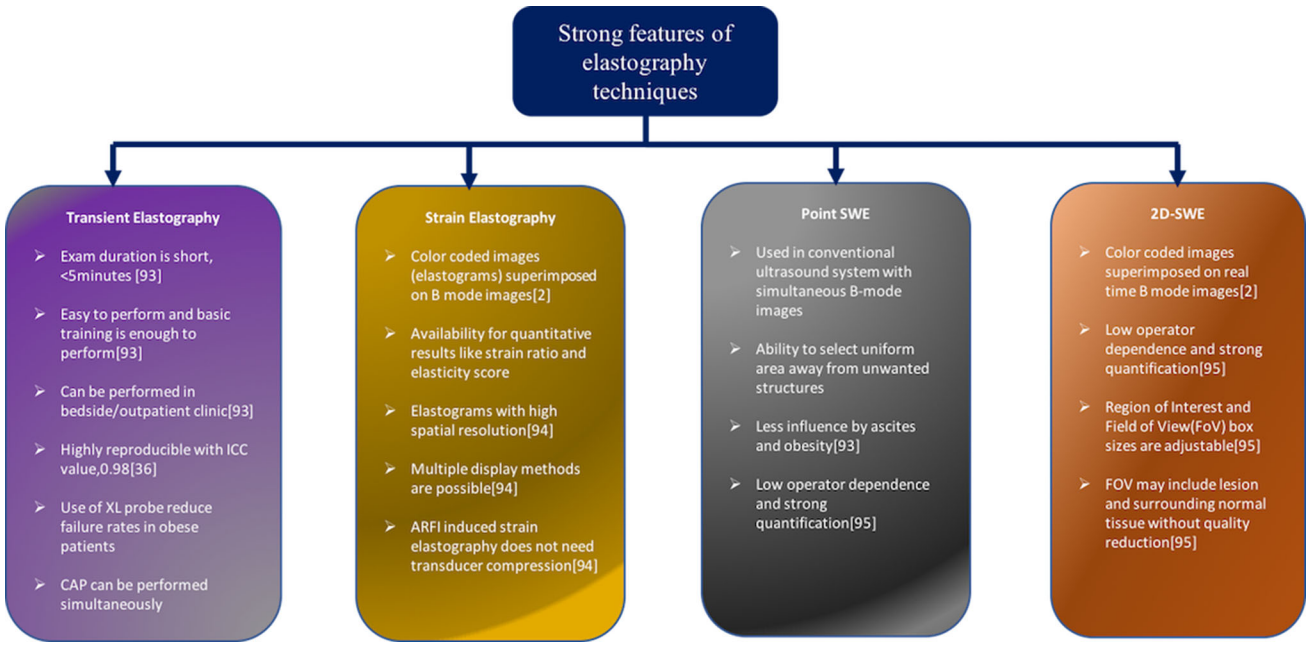

Fig. 10. Strong features of elastography techniques.

Transient elastography

Transient elastography probe can be performed in the spleen in a similar manner to the liver. It is known that TE can successfully detect stiffness of spleen in patients with cirrhosis, which correlates with HVPG which can be predictive for esophageal varices. Spleen stiffness value 3.3 m/s has been proposed as a cut-off value to rule out esophageal varices; however, more studies are needed [92]. In studies comparing TE application in liver and spleen to diagnose portal hypertension, diagnostic performance of liver TE in liver was reported to be higher than splenic TE (AUROC's 0.95 vs. 0.85, respectively) [2]. Use of transient elastography in combination with

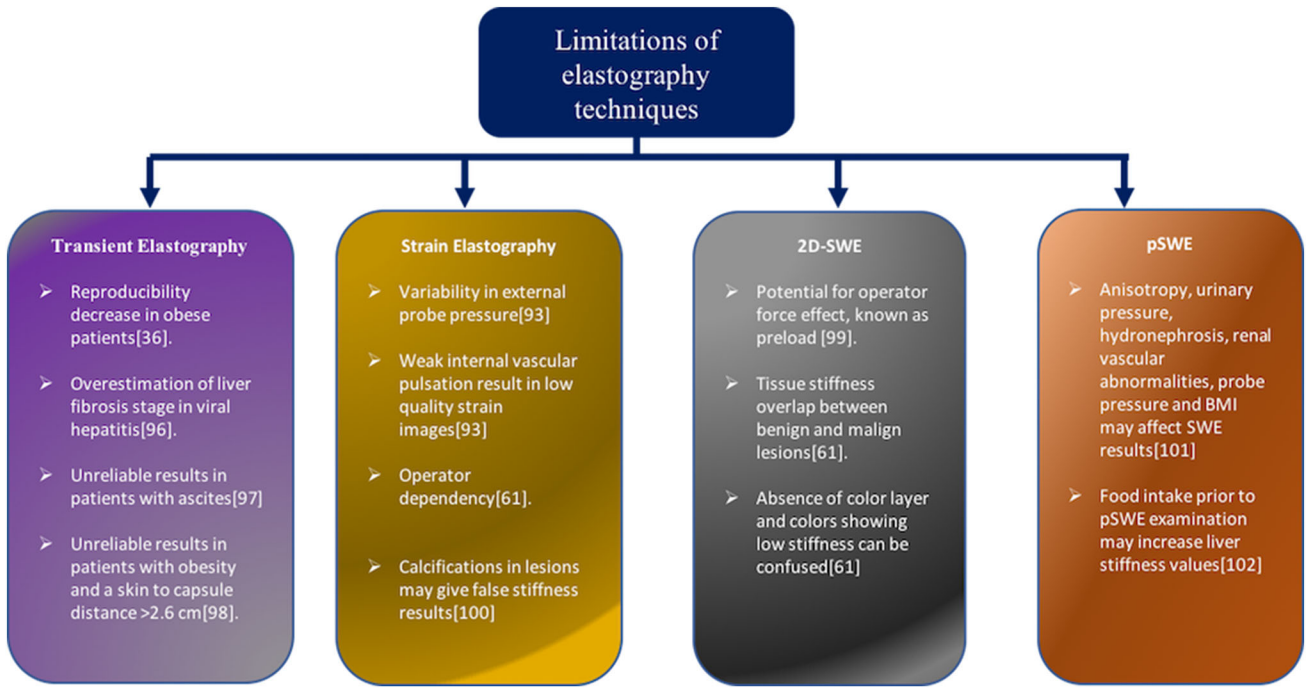

Fig. 11. Limitations of elastography techniques.

conventional ultrasound may help operators to locate the most reliable location [61].

pSWE

pSWE has also been studied in cirrhotic patients. To diagnose clinically significant portal hypertension, pSWE technique was reported to have an AUROC of 0.943 and to detect presence of esophageal varices, pSWE technique was reported to have AUROC of 0.933 [93, 94]. Recently, research groups reported studies with 2D-SWE to predict esophageal varices and portal hypertension [95–97]. Elkrief et al. evaluated the performance of TE and 2D-SWE to detect portal hypertension by measuring liver stiffness and spleen stiffness, and reported higher AUROC value for liver stiffness measurements when compared to spleen stiffness(0.87 vs. 0.64). They also reported superior technical success rate of 2D-SWE when compared to TE, in assessment of liver and spleen stiffness [97]. Although proposed cut-off values of elastography methods to detect portal hypertension or esophageal varices through evaluation of spleen stiffness are similar, more studies are needed to verify these cut-off values.

In this brief review, we have discussed general principles of different elastography technologies and clinical applications of these methods. Summary and classification of all elastographic techniques are indicated in Fig. 9 [10, 11, 15, 16, 27, 31–33, 37–39, 49, 51, 57, 62, 64, 66, 68, 69, 76, 79, 89, 98]. Strong features and limitations of these techniques are summarized in Figs. 10 and 11 [2, 36, 61, 92, 99–107].

Conclusion

Ultrasound elastography comprises a set of techniques that non-invasively measure tissue stiffness. Use of these techniques has blossomed with recognition that many disease processes affect tissue stiffness, providing a new imaging target for assessment of disease biology. In this review, we have provided a brief introduction to the physical concepts that underpin ultrasound elastography, and have discussed several different commercially available ultrasound elastography systems with evidence of their efficacy in different biologic settings. With the help of guidelines, meta-analysis reports, and studies with large study populations, various cut-off values are determined. However, there may be differences between measurements with different ultrasound systems. Researchers and clinicians should liaise with manufacturers regarding their proposed cut-off values for specific elastography applications.

Acknowledgment This work was supported by the NIBIB of the National Institutes of Health under award numbers HHSN268201300071 C and K23 EB020710. The authors are solely responsible for the content and the work does not represent the official views of the National Institutes of Health.

Compliance with ethical standards

Funding Anthony E. Samir's effort was funded by the NIBIB of the National Institutes of Health under award numbers HHSN268201300071 C and K23 EB020710.

Conflict of Interest Anthony E. Samir has received research grants or support from Supersonic Imagine, General Electric, Philips, Toshiba Medical Systems, Hitachi Medical Systems, and Siemens Healthineers. He has also received speaker honoraria from Supersonic Imagine and General Electric and has received consulting fees in related domains from General Electric, Pfizer, Novartis, Bristol Myers Squibb, Jazz Pharmaceuticals, and Parexel. He is a member of the Quantitative Imaging Biomarkers Alliance (QIBA) clinical ultrasound elastography Task Force and is imaging co-chair of the Foundation for the National Institutes of Health Noninvasive Biomarkers of Metabolic Liver Disease (NIMBLE) Biomarkers consortium. He declares no conflict of interest between these various roles and the content of this paper.

Ethical approval This article does not contain any studies with human participants or animals performed by any of the authors.

References

1. Shiina T, Nightingale KR, Palmeri ML, et al. (2015) WFUMB guidelines and recommendations for clinical use of ultrasound elastography: part 1: basic principles and terminology. Ultrasound Med Biol 41(5):1126–1147. https://doi.org/10.1016/j.ultrasmedbio.2015.03.009
2. Sigrist RMS, Liau J, Kaffas AE, Chammas MC, Willmann JK (2017) Ultrasound elastography: review of techniques and clinical applications. Theranostics 7(5):1303–1329. https://doi.org/10.7150/thno.18650
3. Ophir J, Cespedes I, Ponnekanti H, Yazdi T, Li X (1991) Elastography: a quantitative method for imaging the elasticity of biological tissues. Ultrason Imaging 2:111–134
4. Garra BS (2015) Elastography: history, principles, and technique comparison. Abdom Imaging 40(4):680–697. https://doi.org/10.1007/s00261-014-0305-8
5. Itoh A, Ueno E, Tohno E, et al. (2006) Breast disease: clinical application of US elastography for diagnosis. Radiology 239:341–350
6. Zhou J, Zhou C, Zhan W, et al. (2014) Elastography ultrasound for breast lesions: fat-to-lesion strain ratio vs gland-to-lesion strain ratio. Eur Radiol 24:3171–3177. https://doi.org/10.1007/s00330-014-3366-8
7. Barr RG (2010) Real-time ultrasound elasticity of the breast: initial clinical results. Ultrasound 2:61–66. https://doi.org/10.1097/ruq.0b013e3181dc7ce4
8. Guibal A, Boularan C, Bruce M, et al. (2012) Evaluation of shearwave elastography for the characterisation of focal liver lesions on ultrasound. Eur Radiol 23:1138–1149. https://doi.org/10.1007/s00330-012-2692-y
9. Lu Q, Wen JX, Huang BJ, Xue LY, Wang WP (2015) Virtual touch quantification using acoustic radiation force impulse (ARFI) technology for the evaluation of focal solid renal lesions: preliminary findings. Clin Radiol 70(12):1376–1381. https://doi.org/10.1016/j.crad.2015.08.002
10. Samir AE, Dhyani M, Vij A, et al. (2015) Shear-wave elastography for the estimation of liver fibrosis in chronic liver disease: determining accuracy and ideal site for measurement. Radiology 274:888–896. https://doi.org/10.1148/radiol.14140839
11. Samir AE, Allegretti AS, Zhu Q, et al. (2015) Shear wave elastography in chronic kidney disease: a pilot experience in native kidneys. BMC Nephrol. https://doi.org/10.1186/s12882-015-0120-7
12. Hong S, Woo OH, Shin HS, et al. (2017) Reproducibility and diagnostic performance of shear wave elastography in evaluating

breast solid mass. Clin Imaging 44:42–45. https://doi.org/10.1016/j.clinimag.2017.03.022
13. Park SY, Choi JS, Han BK, Ko EY, Ko ES (2017) Shear wave elastography in the diagnosis of breast non-mass lesions: factors associated with false negative and false positive results. Eur Radiol 9:3788–3798. https://doi.org/10.1007/s00330-017-4763-6
14. Boehm K, Salomon G, Beyer B, et al. (2015) Shear wave elastography for localization of prostate cancer lesions and assessment of elasticity thresholds: implications for targeted biopsies and active surveillance protocols. J Urol 193:794–800. https://doi.org/10.1016/j.juro.2014.09.100
15. Samir AE, Dhyani M, Anvari A, et al. (2015) Shear-wave elastography for the preoperative risk stratification of follicular-patterned lesions of the thyroid: diagnostic accuracy and optimal measurement plane. Radiology 277:565–573. https://doi.org/10.1148/radiol.2015141627
16. DeWall RJ, Slane LC, Lee KS, Thelen DG (2014) Spatial variations in Achilles tendon shear wave speed. J Biomech 47:2685–2692. https://doi.org/10.1016/j.jbiomech.2014.05.008
17. Catheline S, Thomas JL, Wu F, Fink MA (1999) Diffraction field of a low frequency vibrator in soft tissues using transient elastography. IEEE Trans Ultrason Ferroelectr Freq Control 4:1013–1019. https://doi.org/10.1109/58.775668
18. Sandrin L, Tanter M, Gennison JL, Catheline S, Fink M (2002) Shear elasticity probe for soft tissues with 1-D transient elastography. IEEE Trans Ultrason Ferroelectr Freq Control 4:436–446
19. Gennisson JL, Deffieux T, Fink M, Tanter M (2013) Ultrasound elastography: principles and techniques. Diagn Interv Imaging 94:487–495. https://doi.org/10.1016/j.diii.2013.01.022
20. Babu AS, Wells ML, Teytelboym OM, et al. (2016) Elastography in chronic liver disease: modalities, techniques, limitations and future directions. Radiographics 36(7):1987–2006. https://doi.org/10.1148/rg.2016160042
21. Castera L, Forns X, Alberti A (2008) Non-invasive evaluation of liver fibrosis using transient elastography. J Hepatol 48:835–847. https://doi.org/10.1016/j.jhep.2008.02.008
22. Sasso M, Beaugrand M, de Ledinghen V, et al. (2010) Controlled attenuation parameter (CAP): a novel VCTE^{TM} guided ultrasonic attenuation measurement for the evaluation of hepatic steatosis: preliminary study and validation in a cohort of patients with chronic liver disease from various causes. Ultrasound Med Biol 36(11):1825–1835. https://doi.org/10.1016/j.ultrasmedbio.2010.07.005
23. Sandrin L, Fourquet B, Hasquenoph JM, et al. (2003) Transient elastography: a new noninvasive method for assessment of hepatic fibrosis. Ultrasound Med Biol 12:1705–1713
24. Bamber J, Cosgrove D, Dietrich C, et al. (2013) EFSUMB guidelines and recommendations on the clinical use of ultrasound elastography. Part 1: basic principles and technology. Ultraschall Med 34:169–184. https://doi.org/10.1055/s-0033-1335205
25. Bercoff J, Tanter M, Fink M (2004) Supersonic shear imaging: a new technique for soft tissue elasticity mapping. IEEE Trans Ultrason Ferroelectr Freq Control 4:396–409
26. Ferraioli G, Tinelli C, Dal Bello B, et al. (2012) Accuracy of real-time shear wave elastography for assessing liver fibrosis in chronic hepatitis C: a pilot study. Hepatology 56:2125–2133. https://doi.org/10.1002/hep.25936
27. Fujimoto K, Kato M, Kudo M, et al. (2013) Novel image analysis method using ultrasound elastography for noninvasive evaluation of hepatic fibrosis in patients with chronic hepatitis C. Oncology 84:3–12. https://doi.org/10.1159/000345883
28. Yada N, Kudo M, Morikawa H, et al. (2013) Assessment of liver fibrosis with real-time tissue elastography in chronic viral hepatitis. Oncology 84:13–20. https://doi.org/10.1159/000345884
29. Koizumi Y, Hirooka M, Kisaka Y, et al. (2011) Liver fibrosis in patients with chronic hepatitis C: noninvasive diagnosis by means of real-time tissue elastography—establishment of the method for measurement. Radiology 2:610–617. https://doi.org/10.1148/radiol.10100319
30. Onur MR, Poyraz AK, Ucak EE, et al. (2012) Semiquantitative strain elastography of liver masses. J Ultrasound Med 7:1061–1067
31. Li Y, Huang YS, Wang ZZ, et al. (2016) Systematic review with meta-analysis: the diagnostic accuracy of transient elastography for the staging of liver fibrosis in patients with chronic hepatitis B. Aliment Pharmacol Ther 43:458–469. https://doi.org/10.1111/apt.13488
32. Ying HY, Lu LG, Jing DD, Ni XS (2016) Accuracy of transient elastography in the assessment of chronic hepatitis C-related liver cirrhosis. Clin Invest Med 39(5):E150–E160
33. Pavlov CS, Casazza G, Nikolova D, Tsochatzis E, Gluud C (2016) Systematic review with meta-analysis: diagnostic accuracy of transient elastography for staging of fibrosis in people with alcoholic liver disease. Aliment Pharmacol Ther 43:575–585. https://doi.org/10.1111/apt.13524
34. Tsochatzis EA, Gurusamy KS, Ntaoula S, et al. (2011) Elastography for the diagnosis of severity of fibrosis in chronic liver disease: a meta-analysis of diagnostic accuracy. J Hepatol 54(4):650–659. https://doi.org/10.1016/j.jhep.2010.07.033
35. Wong VW, Chan HL (2010) Transient elastography. J Gastroenterol Hepatol 11:1726–1731. https://doi.org/10.1111/j.1440-1746.2010.06437.x
36. Fraquelli M, Rigamonti C, Casazza G, et al. (2007) Reproducibility of transient elastography in the evaluation of liver fibrosis in patients with chronic liver disease. Gut 56:968–973
37. Kiani A, Brun V, Lainé F, et al. (2016) Acoustic radiation force impulse imaging for assessing liver fibrosis in alcoholic liver disease. WJG 22(20):4926–4935. https://doi.org/10.3748/wjg.v22.i20.4926
38. Tachi Y, Hirai T, Kojima Y, et al. (2016) Liver stiffness measurement using acoustic radiation force impulse elastography in hepatitis C virus-infected patients with a sustained virological response. Aliment Pharmacol Ther 44:346–355. https://doi.org/10.1111/apt.13695
39. Cao W, Zhou Y, Niu Y, et al. (2017) Quantitative analysis of hepatic toxicity in rats induced by inhalable silica nanoparticles using acoustic radiation force imaging. J Ultrasound Med 36(9):1829–1839. https://doi.org/10.1002/jum.14219
40. Bert F, Stahmeyer JT, Rossol S (2016) Ultrasound elastography used for preventive non-invasive screening in early detection of liver fibrosis. J Clin Med Res 8:650–655. https://doi.org/10.14740/jocmr2625w
41. Hu X, Qiu L, Liu D, Qian L (2017) Acoustic radiation force impulse (ARFI) elastography for non-invasive evaluation of hepatic fibrosis in chronic hepatitis B and C patients: a systematic review and meta-analysis. Med Ultrason 19:23–31. https://doi.org/10.11152/mu-942
42. Cabassa P, Ravanelli M, Rossini A, et al. (2015) Acoustic radiation force impulse quantification of spleen elasticity for assessing liver fibrosis. Abdom Imaging 4:738–744. https://doi.org/10.1007/s00261-014-0306-7
43. Jaffer OS, Lung PFC, Bosanac D, et al. (2012) Acoustic radiation force impulse quantification: repeatability of measurements in selected liver segments and influence of age, body mass index and liver capsule-to-box distance. BJR 85:e858–e863. https://doi.org/10.1259/bjr/74797353
44. Balakrishnan M, Souza F, Muñoz C, et al. (2016) Liver and spleen stiffness measurements by point shear wave elastography via acoustic radiation force impulse. J Ultrasound Med 35:2373–2380
45. Dhyani M, Gee MS, Misdraji J, et al. (2015) Feasibility study for assessing liver fibrosis in paediatric and adolescent patients using real-time shear wave elastography. J Med Imaging Radiat Oncol 59(6):687–694. https://doi.org/10.1111/1754-9485.12388
46. Zheng J, Guo H, Zeng J, et al. (2015) Two-dimensional shear-wave elastography and conventional US: the optimal evaluation of liver fibrosis and cirrhosis. Radiology 275:290–300. https://doi.org/10.1148/radiol.14140828
47. Dhyani M, Grajo JR, Bhan AK, et al. (2017) Validation of shear wave elastography cutoff values on the supersonic aixplorer for practical clinical use in liver fibrosis staging. Ultrasound Med Biol 43:1125–1133. https://doi.org/10.1016/j.ultrasmedbio.2017.01.022
48. Woo H, Lee JY, Yoon JH, et al. (2015) Comparison of the reliability of acoustic radiation force impulse imaging and supersonic shear imaging in measurement of liver stiffness. Radiology 277:881–886. https://doi.org/10.1148/radiol.2015141975
49. Menzilcioglu MS, Duymus M, Citil S, et al. (2015) Strain wave elastography for evaluation of renal parenchyma in chronic kid-

ney disease. BJR 88:20140714–20140716. https://doi.org/10.1259/bjr.20140714
50. Orlacchio A, Chegai F, Del Giudice C, et al. (2014) Kidney transplant: usefulness of real-time elastography (RTE) in the diagnosis of graft interstitial fibrosis. Ultrasound Med Biol 11:2564–2572. https://doi.org/10.1016/j.ultrasmedbio.2014.06.002
51. Cui G, Yang Z, Zhang W, et al. (2014) Evaluation of acoustic radiation force impulse imaging for the clinicopathological typing of renal fibrosis. Exp Ther Med 7(1):233–235
52. Yu N, Zhang Y, Xu Y (2014) Value of virtual touch tissue quantification in stages of diabetic kidney disease. J Ultrasound Med 33(5):787–792. https://doi.org/10.7863/ultra.33.5.787
53. Bob F, Bota S, Sporea I, et al. (2014) Kidney shear wave speed values in subjects with and without renal pathology and inter-operator reproducibility of acoustic radiation force impulse elastography (ARFI): preliminary results. PLoS ONE 9(11):e113761
54. Bota S, Bob F, Sporea I, Sirli R, Popescu A (2015) Factors that influence kidney shear wave speed assessed by acoustic radiation force impulse elastography in patients without kidney pathology. Ultrasound Med Biol 41(1):1–6
55. Wang L (2016) Applications of acoustic radiation force impulse quantification in chronic kidney disease: a review. Ultrasonography 35(4):302–308
56. Hassan K, Loberant N, Abbas N, et al. (2016) Shear wave elastography imaging for assessing the chronic pathologic changes in advanced diabetic kidney disease. Ther Clin Risk Manag 12:1615–1622
57. Barr RG, Nakashima K, Amy D, et al. (2015) WFUMB guidelines and recommendations for clinical use of ultrasound elastography: part 2: breast. Ultrasound Med Biol 41(5):1148–1160. https://doi.org/10.1016/j.ultrasmedbio.2015.03.008
58. Gong X, Xu Q, Xu Z, et al. (2011) Real-time elastography for the differentiation of benign and malignant breast lesions: a meta-analysis. Breast Cancer Res Treat 1:11–18. https://doi.org/10.1007/s10549-011-1745-2
59. Grajo JR, Barr RG (2014) Strain elastography for prediction of breast cancer tumor grades. J Ultrasound Med 33(1):129–134. https://doi.org/10.7863/ultra.33.1.129
60. Zhi H, Xiao XY, Ou B, et al. (2012) Could ultrasonic elastography help the diagnosis of small (≤ 2 cm) breast cancer with the usage of sonographic BI-RADS classification? Eur J Radiol 81(11):3216–3221. https://doi.org/10.1016/j.ejrad.2012.04.016
61. Cosgrove D, Piscaglia F, Bamber J, et al. (2013) EFSUMB guidelines and recommendations on the clinical use of ultrasound elastography. Part 2: clinical applications. Ultraschall Med 34:238–253. https://doi.org/10.1055/s-0033-1335375
62. Li DD, Guo LH, Xu HX, et al. (2015) Acoustic radiation force impulse elastography for differentiation of malignant and benign breast lesions: a meta-analysis. Int J Clin Exp Med 8(4):4753–4761
63. Li G, Li DW, Fang YX, et al. (2013) Performance of shear wave elastography for differentiation of benign and malignant solid breast masses. PLoS ONE. https://doi.org/10.1371/journal.pone.0076322
64. Liu B, Zheng Y, Huang G, et al. (2016) Breast lesions: quantitative diagnosis using ultrasound shear wave elastography-a systematic review and meta-analysis. Ultrasound Med Biol 42:835–847. https://doi.org/10.1016/j.ultrasmedbio.2015.10.024
65. Woo S, Kim SY, Cho JY, Kim SH (2014) Shear wave elastography for detection of prostate cancer: a preliminary study. Korean J Radiol 3:346–355
66. Brock M, von Bodman C, Palisaar RJ, et al. (2012) The impact of real-time elastography guiding a systematic prostate biopsy to improve cancer detection rate: a prospective study of 353 patients. J Urol 187:2039–2043. https://doi.org/10.1016/j.juro.2012.01.063
67. Walz J, Marcy M, Pianna JT, et al. (2011) Identification of the prostate cancer index lesion by real-time elastography: considerations for focal therapy of prostate cancer. World J Urol 29:589–594. https://doi.org/10.1007/s00345-011-0688-x
68. Zheng X, Ji P, Mao H, Hu J (2012) A comparison of virtual touch tissue quantification and digital rectal examination for discrimination between prostate cancer and benign prostatic hyperplasia. Radiol Oncol 46(1):69–74. https://doi.org/10.2478/v10019-011-0026-3
69. Rouvière O, Melodelima C, Dinh AH, et al. (2017) Stiffness of benign and malignant prostate tissue measured by shear-wave elastography: a preliminary study. Eur Radiol 27(5):1858–1866. https://doi.org/10.1007/s00330-016-4534-9
70. Correas JM, Tissier AM, Khairoune A, et al. (2015) Prostate cancer: diagnostic performance of real-time shear-wave elastography. Radiology 275:280–289. https://doi.org/10.1148/radiol.14140567
71. Woo S, Kim SY, Lee MS, Cho JY, Kim SH (2015) Shear wave elastography assessment in the prostate: an intraobserver reproducibility study. Clin Imaging 39(3):484–487. https://doi.org/10.1016/j.clinimag.2014.11.013
72. Sang L, Wang XM, Xu DY, Cai YF (2017) Accuracy of shear wave elastography for the diagnosis of prostate cancer: a meta-analysis. Sci Rep. https://doi.org/10.1038/s41598-017-02187-0
73. Woo S, Suh CH, Kim SY, Cho JY, Kim SH (2017) Shear-wave elastography for detection of prostate cancer: a systematic review and diagnostic meta-analysis. Am J Roentgenol 4:806–814. https://doi.org/10.2214/AJR.17.18056
74. Zhang M, Fu S, Zhang Y, Tang J, Zhou Y (2013) Elastic modulus of the prostate: a new non-invasive feature to diagnose bladder outlet obstruction in patients with benign prostatic hyperplasia. Ultrasound Med Biol 40(7):1408–1413. https://doi.org/10.1016/j.ultrasmedbio.2013.10.012
75. Dighe M, Bae U, Richardson ML, et al. (2008) Differential diagnosis of thyroid nodules with US elastography using carotid artery pulsation. Radiology 248:662–669. https://doi.org/10.1148/radiol.2482071758
76. Bojunga J, Herrmann E, Meyer G, et al. (2010) Real-time elastography for the differentiation of benign and malignant thyroid nodules: a meta-analysis. Thyroid 2010(20):1145–1150. https://doi.org/10.1089/thy.2010.0079
77. Moon HJ, Sung JM, Kim EK, et al. (2012) Diagnostic performance of gray-scale US and elastography in solid thyroid nodules. Radiology 262:1002–1013. https://doi.org/10.1148/radiol.11110839
78. Azizi G, Keller J, Lewis M, et al. (2013) Performance of elastography for the evaluation of thyroid nodules: a prospective study. Thyroid 23:734–740. https://doi.org/10.1089/thy.2012.0227
79. Zhan J, Jin JM, Diao XH, Chen Y (2015) Acoustic radiation force impulse imaging (ARFI) for differentiation of benign and malignant thyroid nodules: a meta-analysis. Eur J Radiol 84(11):2181–2186. https://doi.org/10.1016/j.ejrad.2015.07.015
80. Sporea I, Sirli R, Bota S, et al. (2012) ARFI elastography for the evaluation of diffuse thyroid gland pathology: preliminary results. World J Radiol 4(4):174–178. https://doi.org/10.4329/wjr.v4.i4.174
81. Liu B, Liang J, Zheng Y, et al. (2015) Two-dimensional shear wave elastography as promising diagnostic tool for predicting malignant thyroid nodules: a prospective single-centre experience. Eur Radiol 25:624–634. https://doi.org/10.1007/s00330-014-3455-8
82. Zhang F, Zhao X, Han R, et al. (2017) Comparison of acoustic radiation force impulse imaging and strain elastography in differentiating malignant from benign thyroid nodules. J Ultrasound Med. https://doi.org/10.1002/jum.14302
83. Deng J, Zhou P, Tian SM, et al. (2014) Comparison of diagnostic efficacy of contrast-enhanced ultrasound, acoustic radiation force impulse imaging, and their combined use in differentiating focal solid thyroid nodules. PLoS ONE 3:e90674. https://doi.org/10.1371/journal.pone.0090674
84. Kawada N, Tanaka S (2016) Elastography for the pancreas: current status and future perspective. World J Gastroenterol 22(14):3712–3724. https://doi.org/10.3748/wjg.v22.i14.3712
85. Rustemović N, Kalauz M, Grubelić Ravić K, et al. (2017) Differentiation of pancreatic masses via endoscopic ultrasound strain ratio elastography using adjacent pancreatic tissue as the reference. Pancreas 3:347–351. https://doi.org/10.1097/MPA.0000000000000758
86. Kim SY, Cho JH, Kim YJ, et al. (2017) Diagnostic efficacy of quantitative endoscopic ultrasound elastography for differentiating pancreatic disease. J Gastroenterol Hepatol 5:1115–1122. https://doi.org/10.1111/jgh.13649

87. Iglesias-Garcia J, Domínguez-Muñoz JE, Castiñeira-Alvariño M, Luaces-Regueira M, Lariño-Noia J (2013) Quantitative elastography associated with endoscopic ultrasound for the diagnosis of chronic pancreatitis. Endoscopy 10:781–788. https://doi.org/10.1055/s-0033-1344614
88. Park MK, Jo J, Kwon H, et al. (2014) Usefulness of acoustic radiation force impulse elastography in the differential diagnosis of benign and malignant solid pancreatic lesions. Ultrasonography 33:26–33. https://doi.org/10.14366/usg.13017
89. D'Onofrio M, De Robertis R, Crosara S, et al. (2016) Acoustic radiation force impulse with shear wave speed quantification of pancreatic masses: a prospective study. Pancreatology 16:106–109. https://doi.org/10.1016/j.pan.2015.12.003
90. Pozzi R, Parzanese I, Baccarin A, et al. (2017) Point shear-wave elastography in chronic pancreatitis: a promising tool for staging disease severity. Pancreatology 17:905–910
91. Mateen MA, Muheet KA, Mohan RJ, et al. (2012) Evaluation of ultrasound based acoustic radiation force impulse (ARFI) and eSie touch sonoelastography for diagnosis of inflammatory pancreatic diseases. JOP 13(1):36–44
92. Ferraioli G, Filice C, Castera L, et al. (2015) WFUMB guidelines and recommendations for clinical use of ultrasound elastography: part 3: liver. Ultrasound Med Biol 5:1161–1179. https://doi.org/10.1016/j.ultrasmedbio.2015.03.007
93. Takuma Y, Nouso K, Morimoto Y, et al. (2016) Portal hypertension in patients with liver cirrhosis: diagnostic accuracy of spleen stiffness. Radiology 279(2):609–619. https://doi.org/10.1148/radiol.2015150690
94. Takuma Y, Nouso K, Morimoto Y, et al. (2013) Measurement of spleen stiffness by acoustic radiation force impulse imaging identifies cirrhotic patients with esophageal varices. Gastroenterology 1:92–101. https://doi.org/10.1053/j.gastro.2012.09.049
95. Grgurevic I, Bokun T, Mustapic S, et al. (2015) Real-time two-dimensional shear wave ultrasound elastography of the liver is a reliable predictor of clinical outcomes and the presence of esophageal varices in patients with compensated liver cirrhosis. Croat Med J. 56:470–481. https://doi.org/10.3325/cmj.2015.56.470
96. Kim TY, Kim TY, Kim Y, et al. (2016) Diagnostic performance of shear wave elastography for predicting esophageal varices in patients with compensated liver cirrhosis. J Ultrasound Med 35:1373–1381
97. Elkrief L, Rautou PE, Ronot M, et al. (2015) Prospective comparison of spleen and liver stiffness by using shear-wave and transient elastography for detection of portal hypertension in cirrhosis. Radiology 275(2):589–598. https://doi.org/10.1148/radiol.14141210
98. Kim HG, Park MS, Lee JD, Park SY (2017) Ultrasound elastography of the neonatal brain: preliminary study. J Ultrasound Med 36(7):1313–1319. https://doi.org/10.7863/ultra.16.06079
99. Shiina T (2013) JSUM ultrasound elastography practice guidelines: basics and terminology. J Med Ultrason 40(4):309–323. https://doi.org/10.1007/s10396-013-0490-z
100. Barr Richard G (2017) Principles of elastography. In: Barr RG (ed) *Elastography: a practical approach*, 1st edn. New York: Thieme, pp 6–24
101. Arena U, Vizzutti F, Corti G, et al. (2008) Acute viral hepatitis increases liver stiffness values measured by transient elastography. Hepatology 47:380–384
102. Stevenson M, Lloyd-Jones M, Morgan MY, Wong R (2012) Non-invasive diagnostic assessment tools for the detection of liver fibrosis in patients with suspected alcohol-related liver disease: a systematic review and economic evaluation. Health Technol Assess 16:1–194. https://doi.org/10.3310/hta16040
103. de Ledinghen V, Vergniol J, Foucher J, et al. (2010) Feasibility of liver transient elastography with FibroScan® using a new probe for obese patients. Liver Int 30:1043–1048. https://doi.org/10.1111/j.1478-3231.2010.02258.x
104. Barr RG, Zhang Z (2012) Effects of precompression on elasticity imaging of the breast: development of a clinically useful semiquantitative method of precompression assessment. J Ultrasound Med 31(6):895–902
105. Hong Y, Liu X, Li Z, et al. (2009) Real-time ultrasound elastography in the differential diagnosis of benign and malignant thyroid nodules. J Ultrasound Med 28:861–867
106. Early H, Aguilera J, Cheang E, McGahan J (2017) Challenges and considerations when using shear wave elastography to evaluate the transplanted kidney, with pictorial review. J Ultrasound Med 36(9):1771–1782. https://doi.org/10.1002/jum.14217
107. Popescu A, Bota S, Sporea I, et al. (2013) The influence of food intake on liver stiffness values assessed by acoustic radiation force impulse elastography-preliminary results. Ultrasound Med Biol 39:579–584. https://doi.org/10.1016/j.ultrasmedbio.2012.11.013